THE ASTROPHYSICAL JOURNAL, 495:765–773, 1998 March 10
© 1998. The American Astronomical Society. All rights reserved. Printed in U.S.A.

THE STELLAR AND GASEOUS KINEMATICS IN NGC 253

F. PRADA,[1] C. M. GUTIÉRREZ,[1] AND C. D. MCKEITH[2,3]
Received 1997 March 31; accepted 1997 October 14

ABSTRACT

This paper presents observations made at intermediate spectral and spatial resolutions along the major and minor axes of the starburst galaxy NGC 253. The spectral ranges analyzed are in the region of the stellar Mg I *b* (~5175 Å) line, in the near-IR Ca II triplet (~8550 Å) absorption features, and in the region of the Hα emission line. We compare the shape of the stellar features with those of reference stars and determine the line-of-sight velocity distribution of the stellar component by using a two-dimensional Gaussian decomposition algorithm, and we show for the first time the rotation curve of the stellar component in NGC 253. Comparing the recession velocity curves of the gas and stars, we show that the stellar component has a decoupled kinematics with respect to the gas, displaying a shallower velocity gradient and larger velocity dispersion than the gas in the inner regions. The minor-axis kinematics, together with the kinematics across the central 40″ along the major axis, suggest the presence of a rotating body with a kinematically misaligned axis with respect to the main disk of the galaxy. The asymmetries in the LOS velocity distribution along the minor axis, together with the steep velocity gradient of the gaseous component, suggest a merger scenario as the source of these kinematic signatures. The enclosed mass in the central regions is computed to be $(2.4 \pm 0.5) \times 10^7\ M_\odot$ for a radius of $r = 0\farcs7$ (10 pc). A double gaseous component in the central 6″ is detected from the [S III] λ9069 Å data along the minor axis; this seems to be the signature of a superbubble, due to a supernova rate of 0.05 yr^{-1}.

Subject headings: galaxies: individual (NGC 253) — galaxies: kinematics and dynamics — galaxies: spiral — galaxies: starburst — ISM: dust, extinction

1. INTRODUCTION

The well-known starburst galaxy NGC 253 (e.g., Rieke et al. 1980), classified as type SAB(s)c (de Vaucouleurs et al. 1991), has been the subject of many detailed kinematical studies of its gaseous component. These studies have included long-slit optical spectroscopy (Ulrich 1978; Muñoz-Tuñon, Vilchez, & Castañeda 1993; Arnaboldi et al. 1995, hereafter ARN95), which shows large deviations from noncircular motions. These deviations have been attributed to the outflow of gas in the presence of massive star formation (e.g., Heckman, Armus, & Miley 1990), as well as to heavy obscuration in the central regions (Scoville et al. 1985; Sams et al. 1994). The large amount of extinction seems to be responsible for the steeper rotation curve obtained with near-IR as compared to optical emission lines (Puxley & Brand 1995; Prada et al. 1996b). Infrared measurements are in agreement with the ^{12}CO ($J = 1 - 0$) velocity field derived by Canzian, Mundy, & Scoville (1988). The most complete analysis of the gaseous component in the innermost regions has been performed by Anantharamaiah & Goss (1996, hereafter AG96), using the radio recombination H92α line. They determined a velocity field in the central 150 pc displaying a distinct gaseous kinematics subsystem, rotation in a plane perpendicular to the galactic disk, and an inner region with possible counter-rotation in the plane of the disk. The authors suggest that this result may indicate a secondary bar inside the known primary bar, or, alternatively, may be the signature of a merger or accretion event during the history of the galaxy.

An analysis and comparison of the stellar kinematics with the gaseous motions would be of great interest in determining the nature of this peculiar kinematics found in the central regions of the galaxy. However, up to now, information on the stellar kinematics of NGC 253 has been poor; only the velocity dispersion in the nucleus is known (Lutz & Prada 1995; Oliva et al. 1995). The study presented in this paper reports the results of spectroscopic observations taken in the region of the Mg I *b* line, the Ca II IR triplet stellar features, and the Hα emission line along the major and minor axes of NGC 253.

The paper is structured as follows. Section 2 presents the observations and data reduction, § 3 analyzes the gaseous kinematics and the starbust in the center of the galaxy, and § 4 determines the stellar kinematics and evaluates the enclosed mass in the nuclear region. Section 5 is dedicated to a comparison between the stellar and gaseous kinematics.

2. OBSERVATIONS AND DATA REDUCTION

During several campaigns, we obtained long-slit spectra along the major (P.A. 52°) and minor (P.A. 321°) axes of NGC 253 with the double-arm ISIS spectrograph on the 4.2 m William Herschel Telescope at the Observatorio del Roque de los Muchachos, La Palma, Spain. We used a 1124 × 1124 Tek CCD with 0.″36 pixel^{-1} in the red and blue arms of ISIS, respectively. The spectral dispersion was 0.78 Å pixel^{-1} (with a FWHM = 2 pixels); CuAr and CuNe lamps were used for spectral calibration. The observations are summarized in Table 1. In the observations of 1995 November, the slit was 0.″9 wide, slightly undersampling the ~0.″9 seeing, and was placed along the major axis centered on the apparent optical nucleus. In the observation of 1996 July and August, the slit was placed at the dynamical center given by AG96, with a slit width of 1.″3 and seeing of ~1.″2.

[1] Instituto de Astrofísica de Canarias, 38200 La Laguna, Tenerife, Spain; fprada@iac.es, cgc@iac.es.
[2] Department of Pure and Applied Physics, Queen's University of Belfast, Belfast BT7 1NN, UK.
[3] Deceased.

TABLE 1

OBSERVATIONS

Date	Exposure Time (s)	P.A. (deg)	Spectral Range (Å)	Main features	Template Stars (Spectral type)
1995 Nov.....	1800	52	8300–9100	Ca II, [S III] λ9069	HR 218 (K0 III)
1995 Nov.....	1800	52	4800–5600	Mg I *b*, Hβ, [O III] λ5007	HR 218 (K0 III)
1995 Nov.....	1800	52	6100–6900	Hα, [N II] λ6584, [S II] λλ6717, 6731	HR 218 (K0 III)
1996 Jul	1800	321	8300–9100	Ca II, [S III] λ9069	HD 213947 (K4 III)
1996 Aug	1800	52	8300–9100	Ca II, [S III] λ9069	HD 4388 (G5 III)

The slit was 4′ long in all the runs. In each of these runs, standard stars with spectral types ranging from G5 III to K4 III were also observed. These stars were used as templates to determine the stellar LOS velocity distribution of NGC 253, as explained in the following sections. Standard data reductions, including bias subtraction, flat field correction, and wavelength calibration, were carried out using the IRAF[4] package. The sky lines were subtracted using template spectra from the ends of the slit. A distance of 3.4 Mpc (Sandage & Tammann 1975) for NGC 253 was adopted, yielding a scale of 16.5 pc arcsec^{-1}.

3. THE GASEOUS KINEMATICS AND STAR FORMATION ACTIVITY

Figure 1 shows the gaseous position-velocity curves along the major axis of the galaxy, determined by fitting Gaussian profiles to the [N II] λ6584 Å and [S II] λλ6717, 6731 Å Hα emission lines. The radial velocities are heliocentric, and the zero position for the spatial axis comes from the continuum peak at ∼6500 Å. The systemic velocity of $V_{HEL} = 230 \pm 10$ km s^{-1} is in agreement with previous measurements (e.g., ARN95). The results for the three species are in agreement and show that the center of symmetry for the gas rotation curve is shifted 11″ southwest of the continuum peak, as was first reported by ARN95. Figure 2 compares the [S III] λ9069 Å velocity curve (measured in 1995 November) with the near-IR H_2 $\lambda = 2.1218$ μm position-velocity curve determined by Prada et al. (1996b), and with recent measurements by AG96 using the radio recombination line H92α. There is a good agreement between the three species, except in the southwest of the nucleus, suggesting that this side is especially dusty. This velocity difference has been also found by Prada et al. (1996b), by comparing near-IR data with optical data, and was attributed to an optical depth effect of dust extinction (see § 5).

Figure 3 compares the minor-axis position-velocity curve of the [S III] emission line with the Hα data of Ulrich (1978) and Heckman et al. (1990), and with the measurements taken by AG96 using H92α. The [S III] spectra show two components in the central 6″: the brighter component has the systemic velocity ($V_{HEL} = 230$ km s^{-1}), while the fainter one is blueshifted 140 km s^{-1}. Farther out from the center, our data agree with the Ulrich (1978) data, while the data of Heckman et al. (1990), given only for the southeast, show two components beyond 10″ from the center. We believe that the deeper penetration of the near-IR wavelengths through the dust allow us to see in the equator of the galaxy the two components that Heckman et al. (1990) and Schulz & Wegner (1992) attribute to a starburst-driven superwind at the surface of a cone or bubble. However, our [S III] data

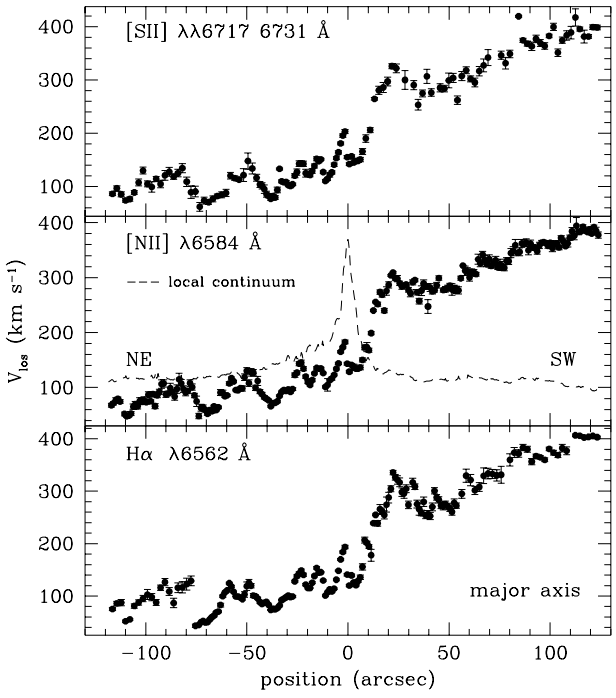


FIG. 1.—Optical gaseous position-velocity curves along the major axis of NGC 253, for the Hα (*bottom panel*), [N II] λ6584 Å (*middle panel*), and [S II] λλ6717, 6731 Å (*top panel*) emission lines. In the middle panel, the relative intensity of the continuum around 6500 Å along the major axis is also plotted.

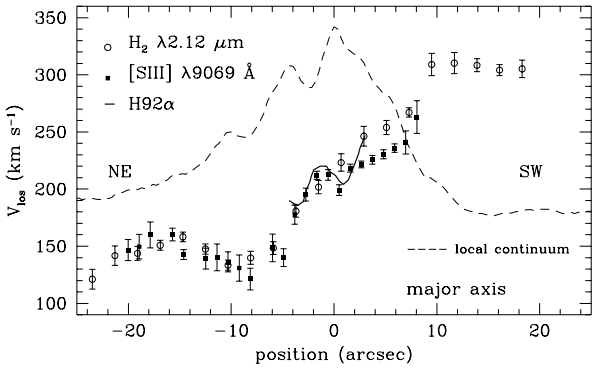


FIG. 2.—Comparison of the position-velocity curves along the major axis of NGC 253 for the [S III] λ9069 Å line, the near-IR H_2 $\lambda = 2.1218$ μm line determined by Prada et al. (1996b), and the measurements by Anantharamaiah & Goss (1996) using the radio recombination line H92α. Dashed lines represent the relative intensity of the continuum around 8750 Å.

[4] IRAF is distributed by National Optical Astronomical Observatories, which is operated by the Association of Universities for Research in Astronomy, Inc., under contract to the National Science Foundation.

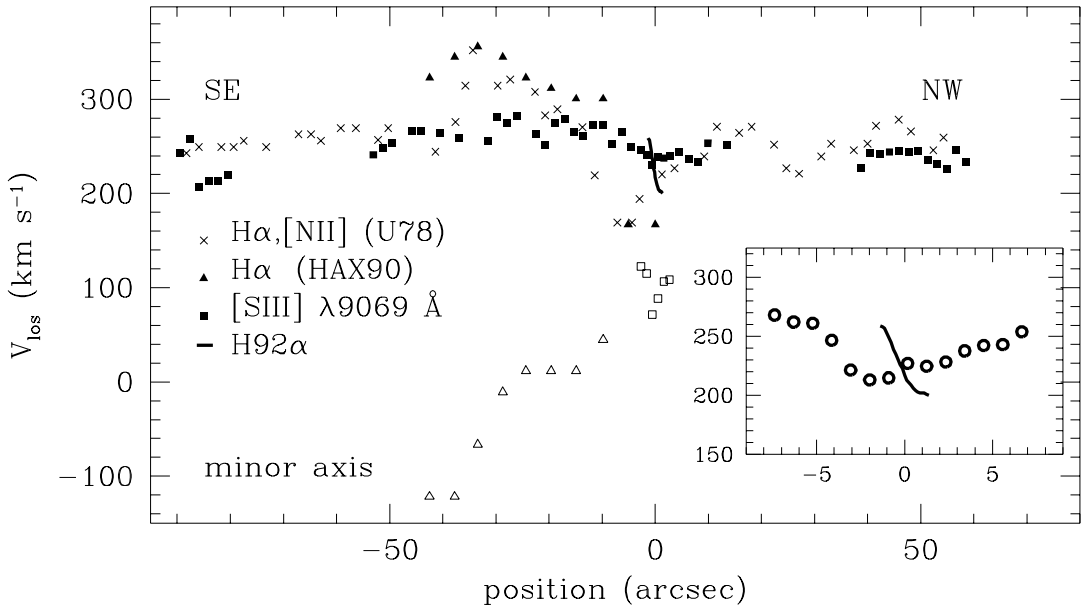


FIG. 3.—Position-velocity curve along the minor axis of NGC 253 for our [S III] λ9069 Å data, the Hα data of Ulrich (1978) and Heckman et al. (1990), and the H92α data of AG96. The central region is plotted magnified at the right. Filled symbols represent the fainter component. Circles in the magnified plot represent a single-Gaussian fit to the [S III] emission lines.

do not agree with the very steep H92α velocity gradient reported by AG96 in the inner 4″ (see Fig. 3); this will be discussed in detail in § 5.

Figure 4 presents the velocity dispersion curve along the major axis of NGC 253 for the optical and the [S III] λ9069 Å emission lines. The optical velocity dispersion curve shows a depression with a minimum value of 65 km s^{-1} at the dynamical center (11″ from the continuum peak), and reaches ∼100 km s^{-1} at 10″ to either side of this. For the [S III] line, the velocity dispersion reaches a value of 85 km s^{-1} at 3.″5 southwest from the continuum peak and decreases slowly toward larger radii. The value of the velocity dispersion at the dynamical center is in agreement with the measurements by Oliva et al. (1995), using Brγ for a central aperture of 4″ × 4″.

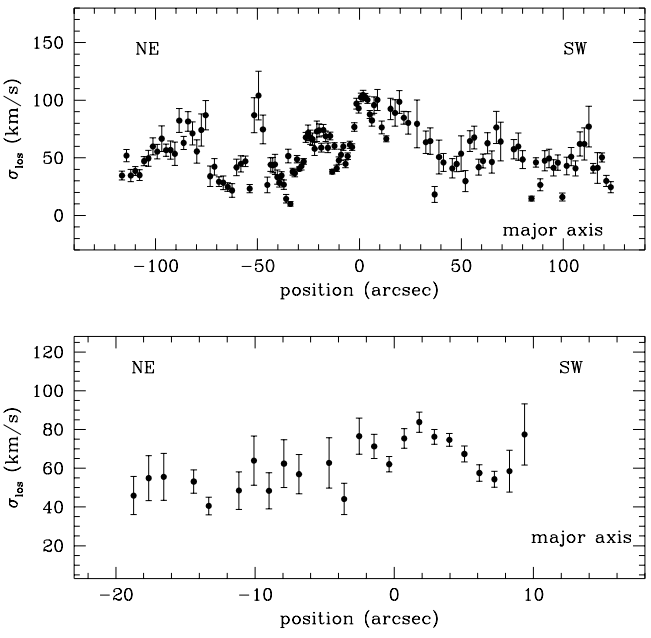


FIG. 4.—Velocity dispersion curve along the major axis of NGC 253 for Hα (*top panel*) and [S III] λ9069 Å (*bottom panel*) emission lines.

The two components present in the [S III] emission lines in the central 4″ along the minor axis of NGC 253 can be interpreted as a large-scale expansion or superbubble arising from supernova (SN) events. The measurement of the gas expansion velocity at the position where the slit intersects the disk of the galaxy, namely the expansion velocity of the superbubble, can be used to constrain the SN rate in the nuclear regions. Colina & Pérez-Olea (1992) consider a SN rate in the nuclear region of 0.05 yr^{-1}, in agreement with the value obtained by Heckman et al. (1990). Using our measurements, an expansion velocity of ∼75 km s^{-1}, deprojected using an inclination of 78.°5 (Pence 1981), and taking the density of the medium in the bubble as $n_0 = 630$ cm^{-3} (Heckman et al. 1990), we estimate a radius of 130 pc for the superbubble in the disk of the galaxy. The radius can be estimated from the equations given by Mac Low & McCray (1988) for the mechanical luminosity of a superbubble, $L_{SN} \sim 3.6 \times 10^{29} n_0\,(\mathrm{cm}^{-3}) R^2(\mathrm{pc}) V^3(\mathrm{km\ s}^{-1})^3$. As the superbubble should be located inside the edge-on nuclear ring of 20″ (330 pc) in diameter reported by ARN95, this introduces a constraint in the SN rate with values much smaller than the one derived by Rieke, Lebofsky, & Walker (1988) and Forbes et al. (1993), who estimate a SN rate of 0.1 or 0.2 yr^{-1}. For this reason, we believe that the average SN rate in the central 300 pc is ∼0.05 yr^{-1}. The value of 0.1–0.2 yr^{-1} could be more local, since it was determined from the presence of few radio sources (Rieke et al. 1988) and the [Fe II] luminosity in the central 50 pc (Forbes et al. 1993) of the galaxy. Finally, it should be mentioned that all the authors agree on a SN rate of ∼0.3 yr^{-1} in the nucleus of M82.

4. THE STELLAR KINEMATICS AND ENCLOSED MASS

We have determined the LOS velocity distribution along the major and minor axes of NGC 253 from the long-slit Mg I *b* (5175 Å) and Ca II IR triplet (8550 Å) absorption

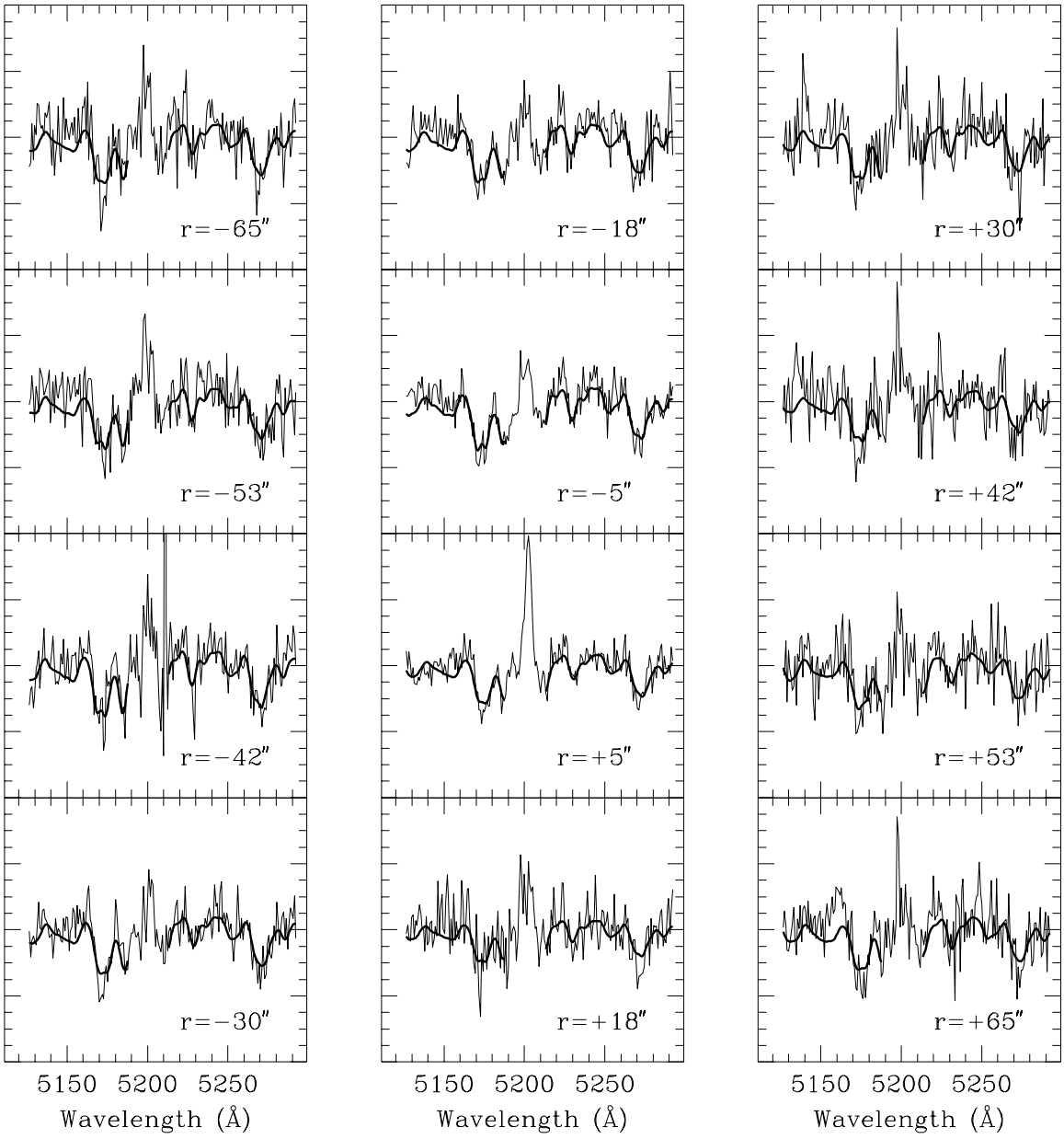


FIG. 5.—Spectra of NGC 253 along the major axis at several positions in a region centered at 5200 Å. The main absorption line is the Mg I *b* feature. The emission at ~5200 Å corresponds to the [N I] doublet gaseous line. Thick lines show the reconvolved spectra obtained using our algorithm (see the text).

spectra by means of a two-dimensional unresolved Gaussian decomposition algorithm. This method has been applied successfully to determine the stellar kinematical structure of NGC 7331 (see Prada et al. 1996a). Basically, this approach considers that the spectrum of the galaxy in a given angular position is the result of a *mean* stellar spectrum broadened by the internal kinematic structure of the galaxy and by the observational/experimental configuration. The intrinsic broadening represents the convolution of this mean stellar spectrum with the LOS velocity distribution. In addition, the instrumental configuration (slit width, etc.) and the atmosphere (seeing) slightly broaden the spectrum in the plane of the detector, introducing correlations between neighboring pixels along both the spectral and the spatial axes. We parametrize the LOS velocity distribution as a sum of two-dimensional Gaussians in the velocity–angular position plane. The dispersion of the Gaussians reflect the resolution in both axes, i.e., spectral and spatial resolution. The dispersions used for the observations presented here are ~2 pixels and ~1.5 pixels in the spectral and spatial axes, respectively, with relative separations of 3 and 2 pixels. The algorithm makes a two-dimensional χ^2 minimization of the difference between the observed and the modeled spectra, using a Newton-Raphson iterative scheme. With respect to the previous algorithm developed by Kuijken & Merrifield (1993), the two-dimensional decomposition takes into account the correlation between adjacent angular positions, as mentioned above. The use of this additional information produces little change in regions of moderate to high signal-to-noise ratio (S/N), but it might be important in regions far away from the galactic center.

The spectral regions analyzed were 5120–5290 Å and 8450–8700 Å along the major and minor axes. For the 1995

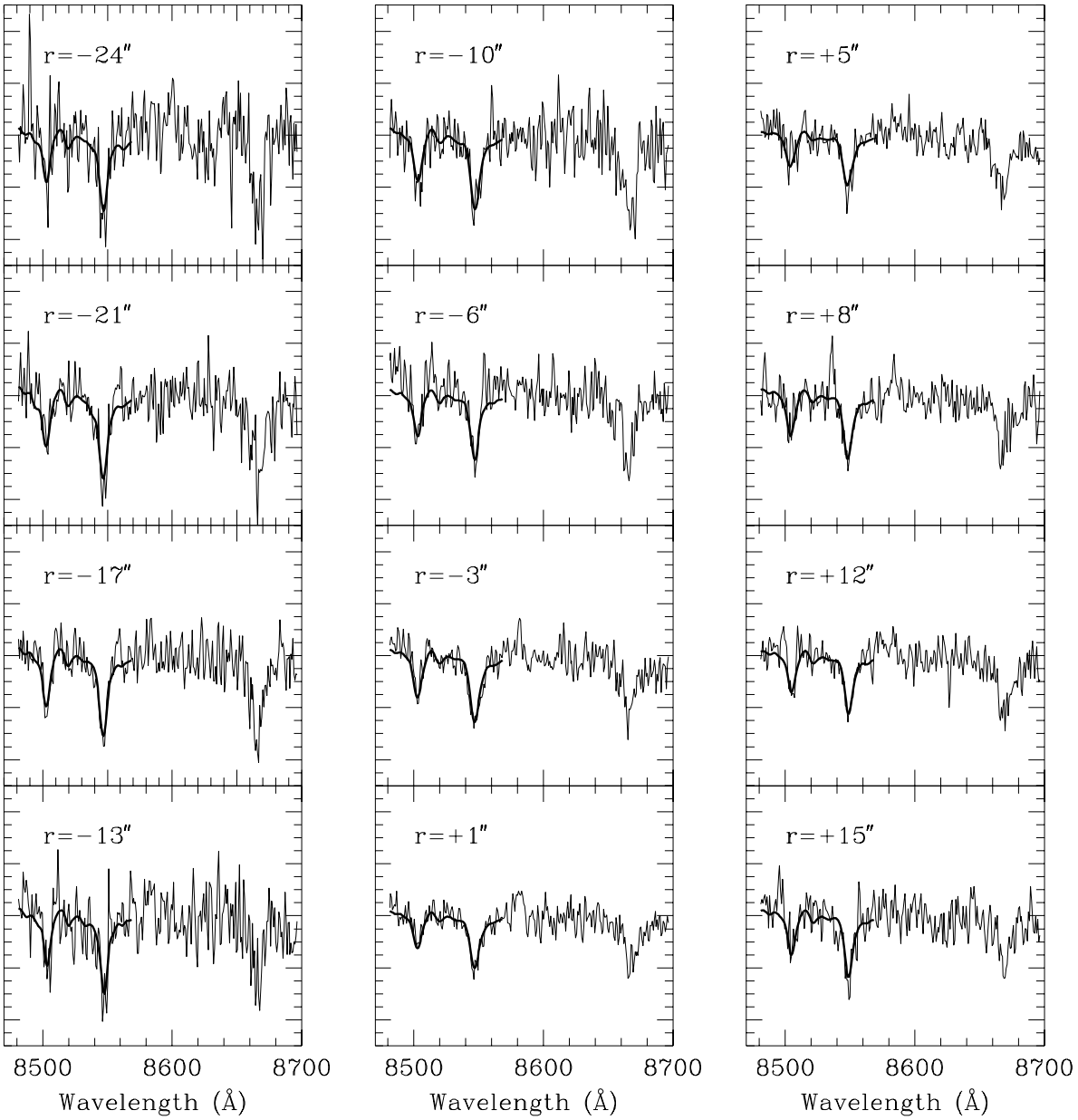


FIG. 6.—Same as Fig. 5, but for the region of the Ca II IR absorption triplet (~8500 Å). Only the two Ca II features at shorter wavelengths (*thick lines*) were used to determine the LOS velocity distribution.

November observations, the K0 giant HR 218 star was used as a velocity template. The K4 III HD 213947 and the G5 III HD 4388 stars were used for the 1996 July and August runs, respectively. Figure 5 shows the spectra in several positions along the major axis in the region of the stellar Mg I *b* feature. The emission feature at ~5200 Å corresponds to the gaseous line [N I] $\lambda\lambda$5198.5, 5200.7 Å. Also plotted are the modeled spectra obtained by convolving the derived LOS velocity distribution with the spectrum of the velocity template (excluding the [N I] feature). Several absorption features, including the main components of the Mg I *b* line, are reconstructed to indicate the reliability of the algorithm and to show that the stellar reference spectra is a good representation of the mean stellar spectrum in the galaxy. Figures 6 and 7 show the equivalent plots in the region around the Ca II IR triplet along the major and minor axes, respectively. For the major axis, the spectra correspond to the 1996 August run. In both cases, the Ca II line at 8662 Å has been excluded from the fit because it appears to be strongly contaminated by sky emission. The reconvolved spectra are very similar, using template stars of types from G5 III to K4 III. Exhaustive analyses of the performance of the algorithm, including Monte Carlo simulations, will be presented in a forthcoming paper (Gutiérrez & Prada 1997).

The LOS velocity distribution along the major axis obtained from the Mg I *b* and Ca II IR triplet are symmetrical and show a single component. Figure 8 shows the radial velocities along the major axis; these have been obtained by fitting a single Gaussian to the LOS velocity distribution. These radial velocities are heliocentric, and the zero position have been chosen from the continuum peak in each case. The Mg I *b* velocity curve goes from −90″ to +120″ from the continuum peak. Overplotted is a linear fit that adequately reproduces the general trend of the curve, having a velocity gradient of 1.7 km s^{-1} $arcsec^{-1}$. Separa-

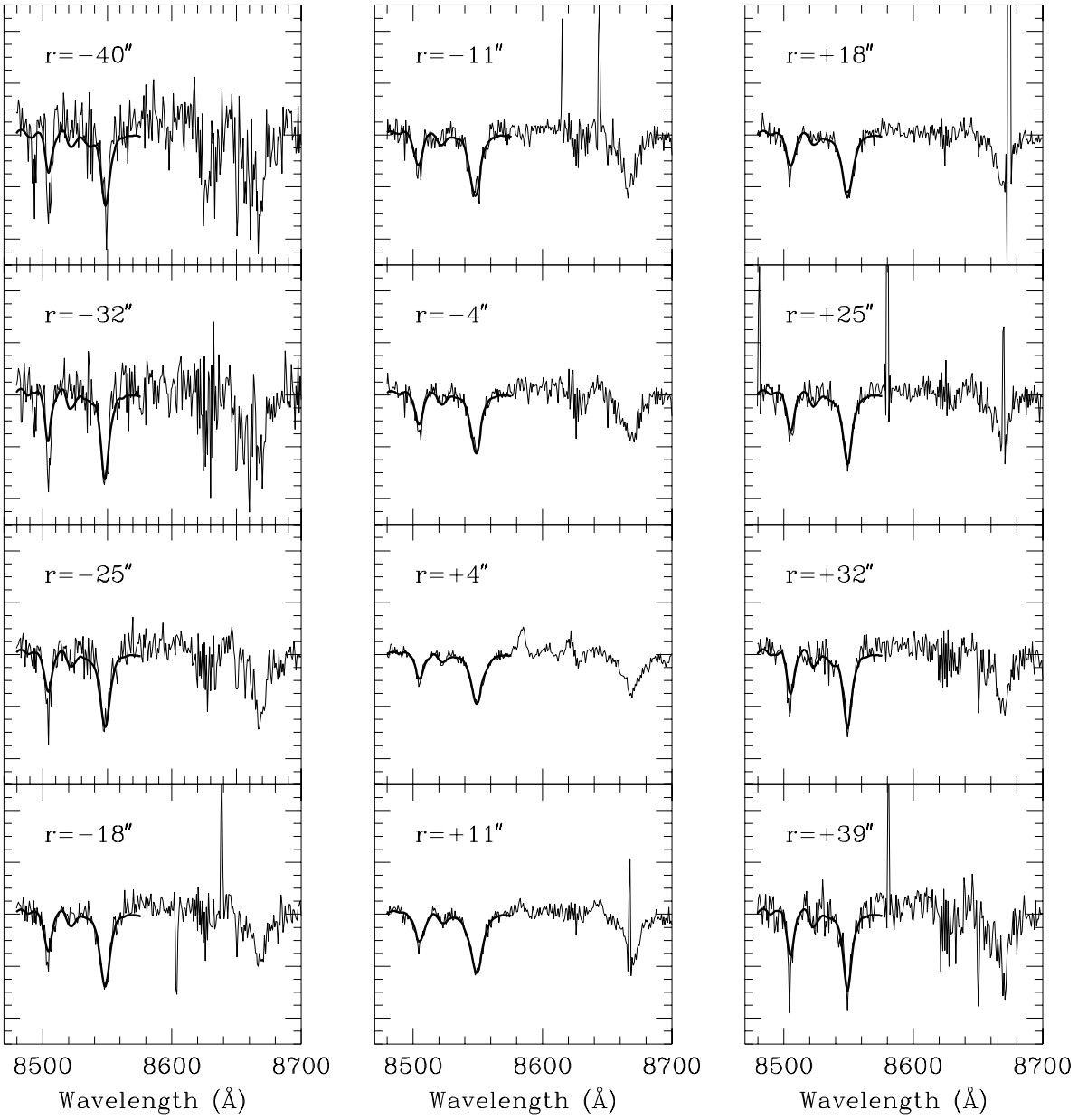


FIG. 7.—Same as Fig. 6, but for Ca II velocities along the minor axis

tion of this trend seems to occur in the region from $\sim +40''$ to $+90''$. For the Ca II triplet, the data of 1996 August allow us to follow the velocity curve over a large spatial range, from $-25''$ to $+25''$ from the continuum peak. Also shown is a fit to the Ca II data of a circular velocity motion (see Bertola et al. 1991). The Ca II velocity curve shows a steeper gradient than the Mg I *b* curve for the southwest side, probably because of the presence of dust in the southwest side of the nucleus (Scoville et al. 1985; Sams et al. 1994).

Figure 9 presents the Ca II IR triplet velocity curve for the minor axis obtained by fitting a single Gaussian to the LOS velocity distribution. The curve shows a velocity gradient that is not expected from circular motions along the main plane of the galaxy. Furthermore, the LOS velocity distribution shows some degree of asymmetry toward the blueshift in the inner $10''$, as shown in Figure 10.

Figure 11 shows the stellar velocity dispersion curve from the Ca II IR data along both axes. The velocity dispersion in the major axis has a value of 90 ± 5 km s^{-1} at $5''$ southwest of the continuum peak, which is in agreement with the values that Oliva et al. (1995) and Lutz & Prada (1995) find using the CO 2.3 μm absorption feature for a central aperture of $4'' \times 4''$. Beyond $\sim 10''$, the velocity dispersion decreases to 70 km s^{-1}. The velocity dispersion along the minor axis reaches a value of 110 ± 20 km s^{-1} in the central $10''$. This can be attributed to the presence of two kinematically distinct components in the inner regions, as revealed by the LOS velocity distribution.

Assuming that the velocity dispersion accounts for all the gravitational support (see McGinn et al. 1989), and following the notation of Gaffney, Lester, & Telesco (1993), the enclosed mass for a given radius is

$$M(r \leq r_o) = \frac{r\sigma^2(r)(A + B + C)}{G}, \qquad (1)$$

where $A = -d \ln n(r)/d \ln (r)$, $B = -d \ln \sigma^2(r)/d \ln r$, and $C = V^2(r)/\sigma^2(r)$. To determine A, we have adopted a surface

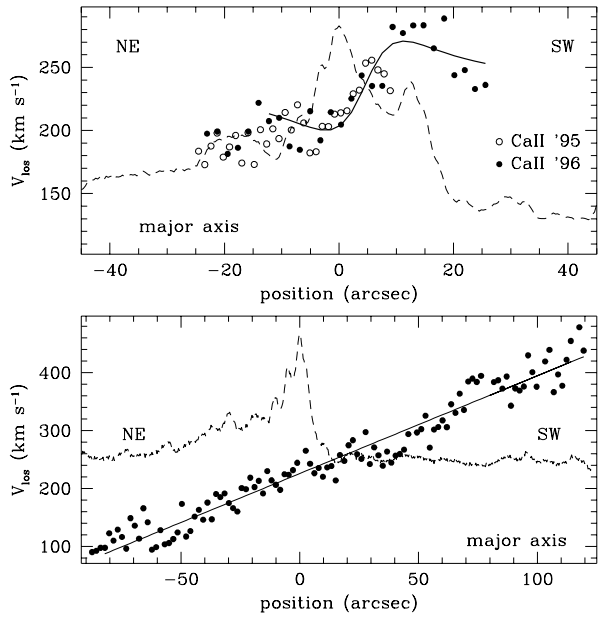


FIG. 8.—Heliocentric radial velocities along the major axis of NGC 253 obtained from the Mg I *b* (*bottom panel*) and Ca II IR triplet (*top panel*) absorption features using the method described in the text. Solid lines represent a circular-motion fit to the Ca II data and a linear fit to the Mg I data, respectively. Dashed lines represent the relative intensity of the continuum at ~5000 and 8750 Å, respectively.

brightness profile of $\mu(r) \propto r^{-0.8 \pm 0.2}$, valid for $1'' \leq r \leq 5''$, determined from near-IR observations (Sams et al. 1994). Hence, we can obtain the flux density $F(r) \propto r^{1.5}$, and $n(r) \propto r^{-1.5}$. B and C were determined from the results shown in Figures 8 and 11. Figure 12 shows the enclosed mass at different radii; for $r = 0''.7$ (10 pc), we obtained an enclosed mass of $(2.4 \pm 0.5) \times 10^7\ M_\odot$. This value is in agreement with the enclosed mass found by Gaffney et al. (1993) for M82, $M(r \leq 7.5\ \mathrm{pc}) = (3 \pm 1) \times 10^7\ M_\odot$.

5. THE DICHOTOMY OF THE STELLAR AND GASEOUS KINEMATICS

A direct comparison of our measurements of the optical stellar Mg I *b* and gaseous (e.g., Hα) position-velocity curves reveals a clear dichotomy between the kinematics of the gas and that of the stars in the central 650 pc of NGC 253 (see Fig. 13). The effects of dust extinction in determining the LOS velocities are very small for the two spectral lines mentioned above, particularly for explaining velocity differences

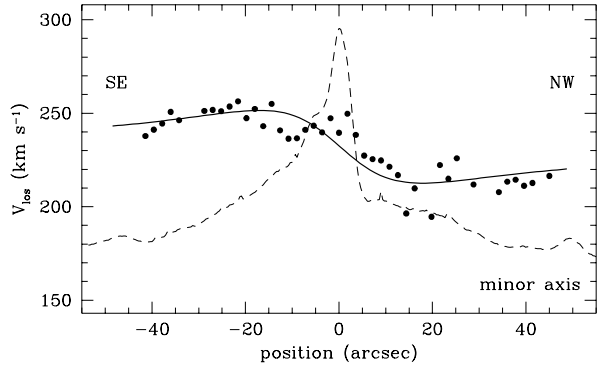


FIG. 9.—Same as Fig. 8, but for Ca II data along the minor axis

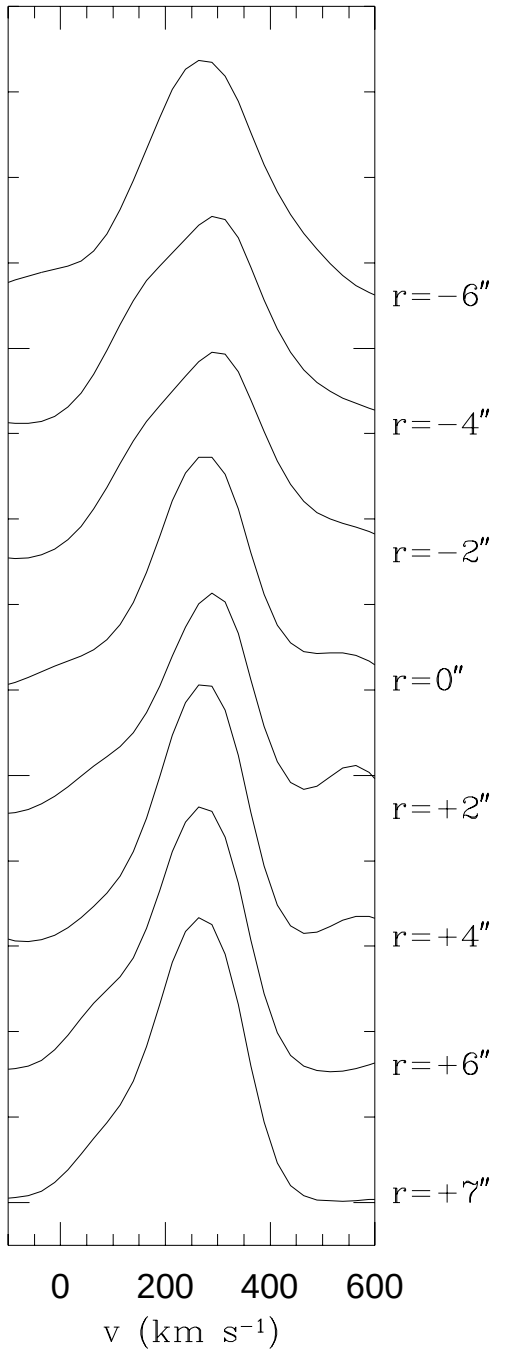


FIG. 10.—Stellar LOS velocity distribution along the minor axis in the central regions of NGC 253. Note a certain degree of asymmetry toward the blueshift.

between gas and stars (see Prada 1995). However, in the southwest side of the nucleus, the heavy obscuration ($A_V \sim$ 30 mag) reveals a steeper velocity gradient for the stellar Ca II near-IR feature, which is shallower than the Hα velocity gradient, the [S III] line, the near-IR emission lines (Puxley & Brand 1995; Prada et al. 1996b), and the radio emission lines (AG96) in this region, but steeper than the Mg I *b* velocity curve.

Adopting the larger wavelength velocity data, i.e., the Ca II IR triplet absorption feature and the emission H92α/H_2 λ2.13 μm lines, as the intrinsic (i.e., extinction-free) stellar and gaseous kinematics of NGC 253, we conclude

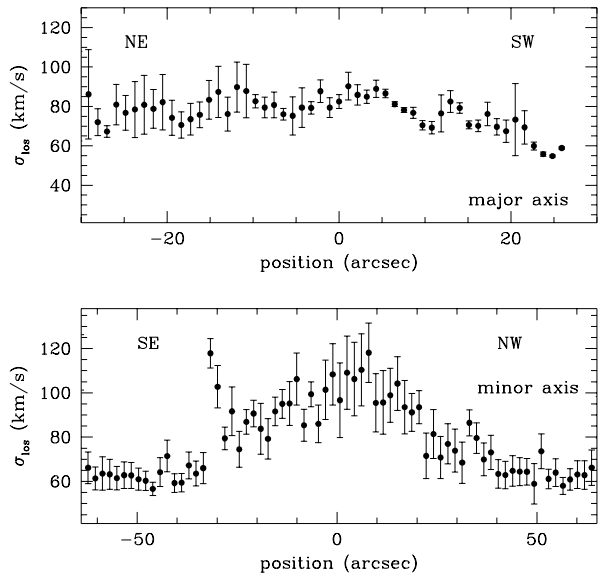


FIG. 11.—Stellar velocity dispersion along the major (*top panel*) and minor (*bottom panel*) axes of NGC 253. Dispersions were obtained according the LOS velocity dispersion determined from the Ca II absorption features (1996 August run).

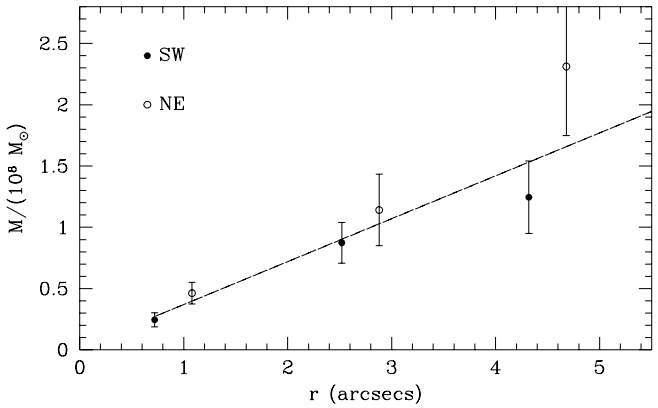


FIG. 12.—Enclosed mass in NGC 253 as a function of radius. Points and error bars represent an estimate assuming that the velocity dispersion accounts for all the gravitational support. Solid line shows a linear fit.

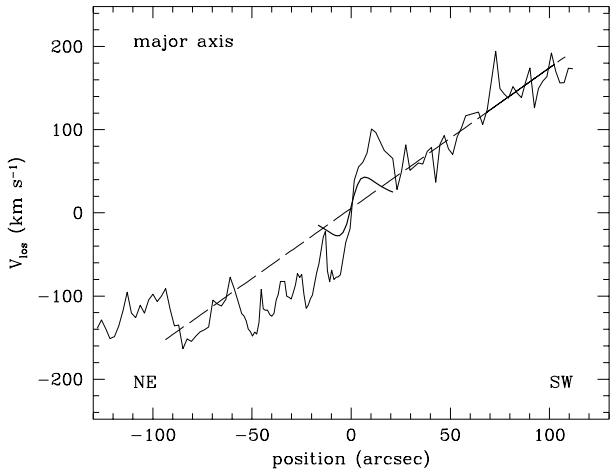


FIG. 13.—Comparison of the velocity-position curves for the gas (*thin line*) and stars (*thick line*) along the major axis of NGC 253, obtained from analysis of the Hα and Ca II lines, respectively. Dashed line is a linear fit to the Mg I *b* stellar curve. The zero position in the spatial axis corresponds to the dynamical center.

that the motions of the stars in the central regions are not coupled with the gas. We think that the velocity difference could be a consequence of the distribution of the gas in a ring. This seems to be confirmed by the high-resolution measurements made by ARN95, who claim the existence of an edge-on nuclear ring based on the presence of an inner Lindblad resonance at 300 pc from the center. They believe that the bar is responsible for the gas fueling the nuclear starburst, and that it will therefore influence the dynamics of the gas in the central regions. This suggests that the gas is distributed in a ring with ongoing star formation and that the stars will trace the kinematics of the regions inside the ring. This suggestion is reinforced by the larger value of the stellar velocity dispersion with respect to the gas, 90 and 65 km s^{-1}, respectively. This difference also occurs in other galaxies, as reported by Terlevich et al. (1990) from observations of the Ca II IR triplet. They find that the only objects with emission lines substantially narrower than their absorption lines are starburst galaxies. Values similar to those for NGC 253 have been found in the nucleus of M82 (Gaffney et al. 1993); in this galaxy as well, the slope of the stellar velocity curve is shallower for the central regions than for the ionized gas, as reported by Gaffney, Lester, & Doppmann (1995). These authors conclude that the stellar peak in M82 may be an older bulge population (Gaffney & Lester 1992; Gaffney et al. 1993); this may also be the case in NGC 253, given the remarkably similarity of the dynamics of M82.

The kinematics along the minor axis of NGC 253 reveals the presence of an ordered motion that appears to be well described by a circular motion with $\Delta V_{max} \sim 40$ km s^{-1} (see Fig. 9). The minor-axis kinematics, together with the kinematics across the central 40″ along the major axis, which has $\Delta V_{max} \sim 70$ km s^{-1}, suggest the presence of a central rotating body with an axis misaligned with respect to the main rotation axis of the galaxy. According to the shape of the LOS velocity distribution, this body might contain a decoupled kinematic component in its center, probably the result of the accretion of material, in the form of either stars or gas, that triggered the starburst.

The counterrotation reported by AG96 in the inner 2″ along the major axis is also present in our [S III] data, although there is a velocity discrepancy in the southeastern regions due to dust extinction, as discussed in § 3. The fact that our [S III] data match the H92α velocity data along the major axis suggests that dust extinction is not very high in the inner 4″ (see Fig. 2). If this is the case, we do not understand the very step velocity gradient found by AG96 along the minor axis. Furthermore, our [S III] minor-axis data show two velocity components. We believe that the discrepancy between the two data sets can be interpreted as follows: by fitting a single Gaussian to the [S III] emission lines, we can match the H92α data by shifting our data 3″.5 northeast. This suggests that the H92α velocity gradient reported by AG96 might represent an artifact arising from the outflow of gas. On the other hand, it could well be that our slit was not placed exactly at the dynamical center, since our positioning error was 1″.25, and that the rapid rotation seen in the H92α data is a kinematic subsystem that might have the same origin as the structure seen in the stellar LOS velocity distribution along the minor axis.

This research is based on observations obtained at the William Herschel Telescope, operated by the Isaac Newton

Group at the Observatorio del Roque de los Muchachos at La Palma of the Instituto de Astrofisica de Canarias. We thank E. Perez and R. F. Peletier for helpful discussions. The spectroscopic observations were performed on service nights in 1995 November and 1996 July and August.

This paper is dedicated to the memory of C. D. McKeith, who contributed much to this work before his untimely death in the summer of 1996.

REFERENCES

Anantharamaiah, K. R., & Goss, W. M. 1996, ApJ, 466, L13 (AG96)
Arnaboldi, M., Capaccioli, M., Cappellaro, E., Held, E. V., & Koribalski, B. 1995, AJ, 110, 199 (ARN95)
Bertola, F., Bettoni, D., Danziger, J., Sadler, E., Sparke, L., & de Zeeuw, T. 1991, ApJ, 373, 369
Canzian, B., Mundy, L., & Scoville, N. Z. 1988, ApJ, 333, 157
Colina, L., & Pérez-Olea, D. 1992, MNRAS, 259, 709
de Vaucouleurs, G., de Vaucouleurs, A., Corwin, H. G., Jr., Buta, R. J., Paturel, G., & Fouqué, P. 1991, Third Reference Catalogue of Bright Galaxies (Berlin: Springer)
Forbes, D. A., Ward, M. J., Rotaciuc, V., Blietz, M., Genzel, R., Drapatz, S., van der Werf, P. P., & Krabbe, A. 1993, ApJ, 406, L11
Gaffney, N. I., & Lester, D. F. 1992, ApJ, 394, 139
Gaffney, N. I., Lester, D. F., & Doppmann, G. 1995, PASP, 107, 68
Gaffney, N. I., Lester, D. F., & Telesco, C. M. 1993, ApJ, 407, L57
Gutiérrez, C. M., & Prada, F. 1997, in preparation
Heckman, T., Armus, L., & Miley, G. 1990, ApJS, 74, 833
Kuijken, K., & Merrifield, M. R. 1993, MNRAS, 264, 712
Lutz, D., & Prada, F. 1995, in IAU Symp. 171, New Light on Galaxy Evolution, ed. R. Bender & R. L. Davies (Dordrecht: Kluwer), 407
Mac Low, M.-M., & McCray, R. 1988, ApJ, 324, 776
McGinn, M. T., Sellgren, K., Becklin, E. E., & Hall, D. N. B. 1989, ApJ, 338, 824
Muñoz-Tuñon, C., Vilchez, J. M., & Castañeda, H. 1993, A&A, 278, 364
Oliva, E., Origlia, L., Kotilainen, J. K., & Moorwood, A. F. M. 1995, A&A, 301, 550
Pence, W. D. 1981, ApJ, 247, 473
Prada, F. 1995, Ph.D. thesis, Queen's University of Belfast
Prada, F., Gutiérrez, C. M., Peletier, R. F., & McKeith, C. D. 1996a, ApJ, 463, L9
Prada, F., Manchado, A., Canzian, B., Peletier, R. F., McKeith, C. D., & Beckman, J. E. 1996b, ApJ, 458, 537
Puxley, P. J., & Brand, P. W. J. L. 1995, MNRAS, 274, L77
Rieke, G. H., Lebofsky, M. J., Thompson, R. I., Low, F. J., & Tokunaga, A. T. 1980, ApJ, 238, 24
Rieke, G. H., Lebofsky, M. J., & Walker, C. E. 1988, ApJ, 325, 679
Sams, B., Genzel, R., Eckart, A., Tacconi-Garman, L., & Hofmann, R. 1994, ApJ, 430, L33
Sandage, A., & Tammann, G. A. 1975, ApJ, 196, 313
Schulz, H., & Wegner, G. 1992, A&A, 266, 167
Scoville, N. Z., Soifer, B. T., Neugebauer, G., Young, J. S., Matthews, K., & Yerka, J. 1985, ApJ, 289, 129
Terlevich, E., Diaz, A. I., & Terlevich, R. 1990, MNRAS, 242, 271
Ulrich, M.-H. 1978, ApJ, 219, 424